Inorganic Chemistry

Article

pubs.acs.org/IC

The Crystal Chemistry of $Ca_{10-y}(SiO_4)_3(SO_4)_3Cl_{2-x-2y}F_x$ Ellestadite

Yanan Fang,*[,†] Clemens Ritter,[‡] and Tim White[†,§]

[†]School of Materials Science & Engineering, Nanyang Technological University, 50 Nanyang Avenue, 639798, Singapore

[‡]Institute Laue-Langevin, 6 rue Jules Horowitz, 38042 Grenoble Cedex 9, France

[§]Centre for Advanced Microscopy, Sullivan's Creek Road, Australian National University, Canberra ACT 0200 Australia

Supporting Information

ABSTRACT: Fluor-chlorellestadite solid solutions $Ca_{10}(SiO_4)_3(SO_4)_3Cl_{2-x}F_x$, serving as prototype crystalline matrices for the fixation of hazardous fly ash, were synthesized and characterized by powder X-ray and neutron diffraction (PXRD and PND), transmission electron microscopy (TEM), and Fourier transform infrared spectroscopy (FTIR). The lattice parameters of the ellestadites vary linearly with composition and show the expected shrinkage of unit cell volume as fluorine (IR = 1.33 Å) displaces chlorine (IR = 1.81 Å). FTIR spectra indicate little or no OH^- in the solid solutions. All compositions conform to $P6_3/m$ symmetry where F^- is located at the 2*a* (0, 0, $^1/_4$) position, while Cl^- is displaced out of the 6*h* Ca(2) triangle plane and occupies 4*e* (0, 0, *z*) split positions with *z* ranging from 0.336(3) to 0.4315(3). Si/S randomly occupy the 6*h* tetrahedral site. Ellestadites rich in Cl ($x \leq 1.2$) show an overall deficiency in halogens (<2 atom per formula unit), particularly Cl as a result of $CaCl_2$ volatilization, with charge balance achieved by the creation of Ca vacancies ($Ca^{2+} + 2Cl^- \rightarrow \square_{Ca} + 2\square_{Cl}$) leading to the formula $Ca_{10-y}(SiO_4)_3(SO_4)_3Cl_{2-x-2y}F_x$. For F-rich compositions the vacancies are found at Ca(2), while for Cl-rich ellestadites, vacancies are at Ca(1). It is likely the loss of $CaCl_2$ which leads tunnel anion vacancies promotes intertunnel positional disorder, preventing the formation of a $P2_1/b$ monoclinic dimorph, analogous to that reported for $Ca_{10}(PO_4)_6Cl_2$. Trends in structure with composition were analyzed using crystal-chemical parameters, whose systematic variations served to validate the quality of the Rietveld refinements.

1. INTRODUCTION

Structural adaptation in apatites makes them suitable for environmental remediation,[1] catalysis and energy production,[2] as well as the traditional biomedical uses of bone and teeth replacement.[3,4] Optimization of chemically substituted apatites for these applications demands a comprehensive understanding of their chemical and crystallographic properties. Apatites also show promise as waste form ceramics for the immobilization of incinerator fly ash,[5] however our crystallochemical knowledge is presently insufficient to tailor formulations and predict durability reliably.

Ellestadite is a silicon- and sulfur-rich member of the apatite family of the general composition $Ca_{10}(SiO_4)_{3-x/2}(PO_4)_x(SO_4)_{3-x/2}(F/Cl/OH)_2$,[6] when described in $P6_3/m$ symmetry the unit cell contains two formula units and the crystallochemical representation is $[A(1)]_4[A(2)]_6(BO_4)_6X_2$ (*A* = Ca, *B* = Si/P/S, and *X* = F/Cl/OH) (Figure 1a). The topology is zeolite-like, in that a framework composed of $Ca(1)O_6$ metaprism columns, corner-connected to $(Si/P/S)O_4$ tetrahedra, creates tunnels perpendicular to the basal plane that enclose $Ca(2)O_5(F/Cl/OH)$ polyhedra. While phosphate apatites are generally hexagonal, the symmetry of ellestadite remains controversial. In a single crystal X-ray diffraction study of a specimen from Chichibu Mine, Sudarsanan[7] assigned the space group as $P2_1/m$ that differentiated the substitutional positions of SO_4 and SiO_4 for PO_4 groups. This ordering was incomplete and the presence of trace elements obscured an unambiguous solution. In another mineral study, Organova et al.[8] reported $P2_1$ symmetry which yields three independent $(Si/P/S)O_4$ tetrahedral sites and two discrete CaO_6 metaprisms (Figure 1b). Saint-Jean and Sweden[9] synthesized chlorellestadite under different conditions (annealing time, temperature, $CaCl_2$ content), but only the hexagonal phase was observed. Thus, the precise arrangement of the metalloids in ellestadite and its symmetry remain in question, and may be dependent on petrogenesis or fabrication conditions.

The scope of this work was to synthesize and characterize fluor-chlorellestadites, $Ca_{10}(SiO_4)_3(SO_4)_3Cl_{2-x}F_x$, as simplified surrogates for apatite derived from the stabilization of certain solid waste ashes, and establish the continuity of the solid solution series. The role of substituted fluorine in promoting higher chemical stability (e.g., reducing dental caries[10]) and thermal resistance (e.g., higher melting points[11]) is well-known, with the interaction between fluorine and chlorine capable of attenuating these properties. Commonly, the fluor- and chlorellestadites are regarded as isostructural, although the halides reside at different locations along the *c*-axis anion tunnels. In the synthetic fluorellestadite ($P6_3/m$) endmember, F^- at (0, 0, $^1/_4$ and 0, 0, $^3/_4$) lies in the center of a Ca(2) triangle on the mirror planes at $z = {}^1/_4$ and $z = {}^3/_4$.[12] In the corresponding chlorellestadite endmember, Cl^- cannot fit into the Ca(2) triangle (ionic radii for $^{VI}F^-$ = 1.33 Å and $^{VI}Cl^-$ = 1.81 Å[13]), and statistically occupies (0, 0, *z*) sites, ~1.1 Å above or below the mirror plane.[9] In the case of natural hydroxyellestadite, Sudarsanan[7] refined separate sites for OH^- (0, 0, 0.2033), F^- (0, 0, $^1/_4$), and Cl^- (0, 0, 0.3644) in $P2_1/m$ with site occupancies of 0.806(9), 0.15(6), and 0.092(5) respectively.

Received: August 3, 2011
Published: November 23, 2011

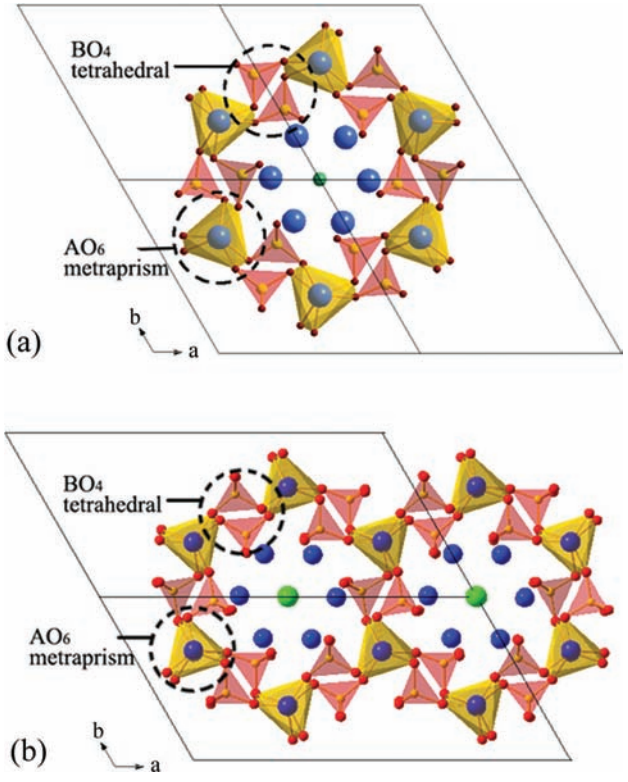

Figure 1. (a) Hexagonal $P6_3/m$ apatite structure of $[A_4][A_6](BO_4)_6X_2$. The AO_6 metraprisms contain calcium, while the BO_4 tetrahedra accommodate phosphorus, sulfur and silicon. The tunnel contains fluorine, chlorine or oxygen without intertunnel correlation. (b) Monoclinic $P2_1$ apatite structure of $[A_4][A_6](BO_4)_6X_2$. The AO_6 metraprisms contain calcium while the BO_4 tetrahedra accommodate phosphorus, sulfur and silicon. The tunnels contain fluorine, chlorine, or oxygen where intertunnel correlation leads a doubling of the *b*-axis metric.

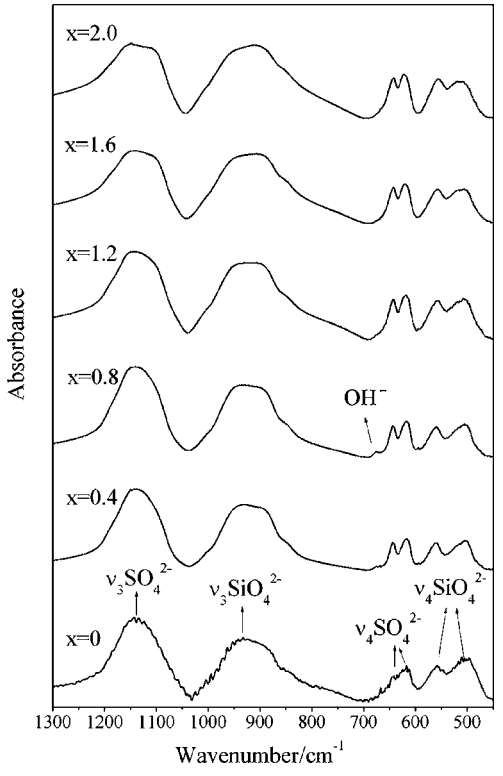

Figure 2. Expanded views of FT-IR spectra for the fluor-chlorellestadite solid solution. (x in $Ca_{10}(SiO_4)_3(SO_4)_3Cl_{2-x}F_x$).

Onac et al.[14] suggested minor substitutions of F^- and Cl^- at the same site as OH^- in a hydroxylellestadite ($P6_3/m$) from Cioclovina Cave, Romania, although at the unit cell scale this is unlikely to satisfy bond valence sum criteria. In general, the interaction between F^- and Cl^-, and the influence on $Ca_{10}(SiO_4)_3(SO_4)_3X_2$ (where X = F, Cl) ellestadite require clarification. Two reports concerning the structural adjustments and anion tunnel accommodation in binary solid solutions of (Cl, OH) or (F, OH) in calcium phosphate apatite $Ca_{10}(PO_4)_6X_2$, and ternary solutions of (F, Cl, OH)[15,16] have appeared, but less is known about the (F, Cl) system. Mackie and Young[17] studied two fluor-chlorapatite compositions with F/(F+Cl) ratios of 0.17 and 0.41, and included a second fluorine site in addition to that on the mirror plane. Hughes et al.[18] suggested that OH^- may be an essential component in stabilizing natural fluor-chlorapatite solid solutions. The presence of a miscibility gap in natural gem-grade apatite from Brazil has been described by Ferraris et al.,[19] where atomic scale studies by high-resolution and analytical TEM revealed the phase separation of fluorine-enriched and chlorine-enriched phosphate apatite domains from ellestadite in the nanoscale.

An understanding of the structural atomic arrangement and physical-chemical properties of fluor-chlorellestadite is an essential prerequisite for formulating synthetic ellestadites for hazardous waste immobilization. To this end, infrared spectroscopy, powder X-ray and neutron diffraction, and transmission electron microscopy were used here to examine the structural adaptations and nanometric properties of synthetic fluor-chlorellestadite.

2. EXPERIMENTAL METHODS

2.1. Synthesis. $Ca_{10}(SiO_4)_3(SO_4)_3Cl_{2-x}F_x$ (x = 0, 0.4, 0.8, 1.2, 1.6, and 2) were synthesized by solid-state reaction. The starting materials were prepared by preheating $CaCO_3$ (Merck, p.a.) at 1000 °C for 12 h; SiO_2 (Sigma-Aldrich, 99.99%) and $CaSO_4{\cdot}2H_2O$ (Merck, p.a.) at 600 °C for 4 h; and $CaCl_2{\cdot}2H_2O$ (Riedel-de Haën, puriss.) at 400 °C for 4 h. Stoichiometric mixtures of CaO, $CaSO_4$, SiO_2, $CaCl_2$, and CaF_2 were manually ground with acetone and calcined at 900 °C for 5 h in an alumina crucible, then reground and sintered at 950 °C for a further 9 h.

2.2. Crystallographic Characterization. Powder X-ray diffraction (PXRD) and neutron diffraction (PND) were combined for structural characterization. PXRD measurements were performed for phase identification and mass balance using a Bruker D8 high-resolution X-ray powder diffractometer (Cu−Kα radiation) operated at 40 kV and 40 mA. Scans were collected from 8° to 140° with a step size of 0.01° and a dwell time per step of 1 s. All specimens were spiked with standard silicon (10 wt %, NIST660a, a = 5.40825 Å) to determine the unit cell constants absolutely. Powder neutron diffraction patterns were acquired at the Institute Laue-Langevin (ILL) Grenoble (France) using the high resolution D1A diffractometer with a wavelength of 1.3894 Å, a 2-theta range of 0° to 150° and scan step of 0.05° at room temperature. The diffractometer is equipped with a focusing Ge monochromator set at a takeoff angle of 123°, and 25 standard ^{3}He counter detectors. Approximately 2 g of ellestadite was loaded into a 9 mm diameter cylindrical sample container that was rotated during acquisition.

The structure refinements were carried out by the Rietveld method using TOPAS[20] with a pseudo-Voigt peak shape profile and a starting model using the atomic positions of $Ca_{10}(SiO_4)_3(SO_4)_3Cl_2$ in hexagonal $P6_3/m$.[21] Although monoclinic forms have been documented, such occurrences were not observed in this study, as 2b

dx.doi.org/10.1021/ic201673r | *Inorg. Chem.* 2011, 50, 12641−12650

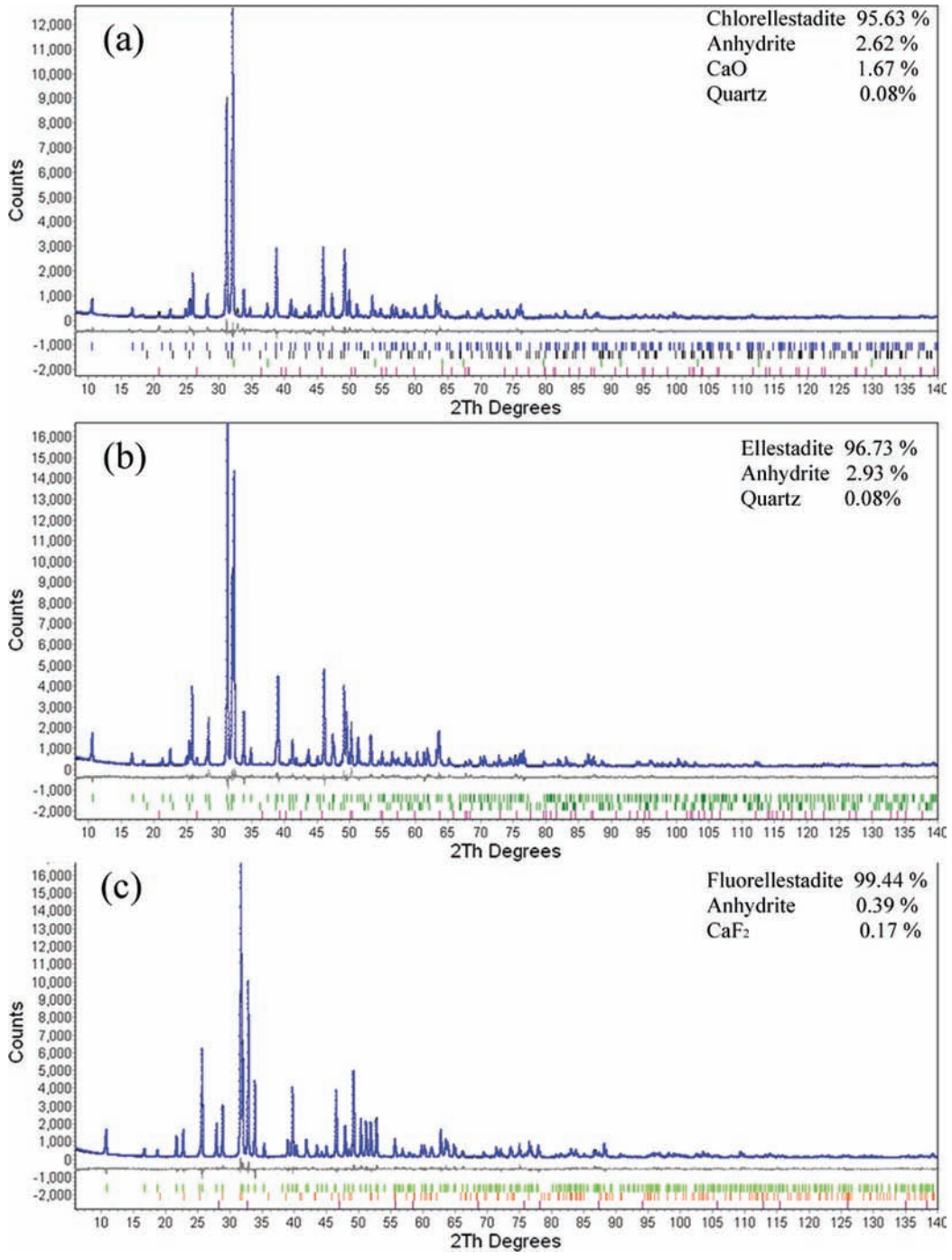

Figure 3. Rietveld fitting pattern for (a) $x = 0$, (b) $x = 0.4$ and (c) $x = 2$. (x in $Ca_{10}(SiO_4)_3(SO_4)_3Cl_{2-x}F_x$) Lines and dots denote observed and calculated profile intensities, respectively. Short vertical bars represent Bragg reflection positions. The difference (observed − calculated) is plotted below.

superstructure reflections were absent, and improvements in R values with lower symmetries ($P2_1/m$; $P2_1$) were insignificant. For each data set, a five-coefficient Chebychev function and $1/x$ background, a peak shift, a zero error, unit cell parameters, and crystal size were refined sequentially with temperature displacement parameters and occupation factors of each atomic site kept constant. After several refinement cycles, the calcium positions (Ca(1) and Ca(2)) were released, followed by the silicon/sulfur and oxygen positions. The mole ratio of Si:S at the tetrahedral site was fixed at 1:1. The oxygen sites were fully tenanted, while the occupancies of calcium, chlorine and fluorine were allowed to vary. For nonstoichiometric ellestadites, the occupancy factors of Ca and Cl were constrained to maintain charge balance (see Discussion and Table 3). Isotropic temperature displacement parameters for all atoms were refined in Ca(1)/Ca(2)/Cl/F and Si/S/O(1)/O(2)/O(3) groups to the same value. The refinement cycles were terminated when convergence was reached. Scattering lengths of 0.4700, 0.4149, 0.2847, 0.5803, 0.5654, and 0.9577×10^{-12} cm were used for Ca, Si, S, O, F, and Cl, respectively.[22] Difference-Fourier maps were generated using Jana2006,[23] specifically to examine the location of anion scattering centers in the tunnels. The $Ca(1)O_6$ metaprism twist angle (φ) was calculated according to the method of White and Dong[24] for cystallochemical diagnosis, and verify trends bond angles as a function of composition. To objectively assess the reliability of the Rietveld refinements singular value decomposition as implemented in

dx.doi.org/10.1021/ic201673r | Inorg. Chem. 2011, 50, 12641–12650

Table 1. Lattice Parameters and Crystallographic Data for $Ca_{10}(SiO_4)_3(SO_4)_3Cl_{2-x}F_x$[a]

x	0	0.4	0.8	1.2	1.6	2.0
space group	$P6_3/m$	$P6_3/m$	$P6_3/m$	$P6_3/m$	$P6_3/m$	$P6_3/m$
a (Å)	9.6702(3)	9.6239 (3)	9.5772(2)	9.5312(2)	9.5064(2)	9.4486(1)
c (Å)	6.8543(3)	6.87749 (3)	6.8950(1)	6.9181(2)	6.9263(1)	6.9426(1)
volume (Å^3)	555.09(4)	551.64(2)	547.70(3)	544.27(3)	542.09(2)	536.77(2)
φ(deg)	19.9_2	20.4_4	21.8_9	22.0_1	22.6_3	24.1_5
R_{wp}	5.62%	4.30%	5.43%	6.72%	6.74%	8.55%
R_p	4.28%	3.37%	4.21%	5.24%	5.05%	6.48%
GOF	0.84	0.58	0.61	0.73	0.74	0.89
Ca(1), 4*f* ($^1/_3$, $^2/_3$, *z*)						
z	−0.0013(1)	0.0009(4)	0.0010(5)	0.0037(9)	0.0028(4)	0.0026(1)
B (Å^2)	1.88(6)	1.85(7)	1.81(6)	1.52(7)	1.52(7)	1.46(7)
Ca(2), 6*h* (*x*, *y*, $^1/_4$)						
x	0.2603(5)	0.2562(4)	0.2497(3)	0.2435(1)	0.2420(3)	0.2390(4)
y	0.0012(6)	−0.0017(3)	−0.0068(4)	−0.0101(4)	−0.0094(3)	−0.0088(2)
B (Å^2)	1.88(6)	1.85(7)	1.81(6)	1.52(7)	1.52(7)	1.46(7)
Si/S, 6*h* (*x*, *y*, $^1/_4$)						
x	0.4062(1)	0.4045(2)	0.4008(2)	0.3996(1)	0.3996(1)	0.3980(1)
y	0.3767(1)	0.3755(4)	0.3721(1)	0.3705(2)	0.3706(1)	0.3704(3)
B (Å^2)	1.84(3)	2.00(4)	1.79(3)	1.60(4)	1.52(4)	1.51(3)
O(1), 6*h* (*x*, *y*, $^1/_4$)						
x	0.3368(5)	0.3359(4)	0.3331(1)	0.3296(4)	0.3302(4)	0.3245(3)
y	0.4900(4)	0.4902(8)	0.4885(1)	0.4859(4)	0.4870(3)	0.4843(3)
B (Å^2)	1.84(3)	2.00(4)	1.79(3)	1.60(4)	1.52(4)	1.51(3)
O(2), 6*h* (*x*, *y*, $^1/_4$)						
x	0.5907(1)	0.5898(1)	0.5872(1)	0.5867(1)	0.58724(8)	0.5868(3)
y	0.4676(4)	0.4667(3)	0.4651(2)	0.4662(4)	0.4660(3)	0.4676(3)
B (Å^2)	1.84(3)	2.00(4)	1.79(3)	1.60(4)	1.52(4)	1.51(3)
O(3), 12*i* (*x*, *y*, *z*)						
x	0.3549(4)	0.3512(1)	0.3483(1)	0.3443(4)	0.3426(3)	0.3410(3)
y	0.2675(3)	0.2647(2)	0.2628(1)	0.2599(3)	0.2587(2)	0.2573(2)
z	0.0684(3)	0.0701(1)	0.0688(1)	0.0700(2)	0.0712(2)	0.0717(2)
B (Å^2)	1.84(3)	2.00(4)	1.79(3)	1.60(4)	1.52(4)	1.51(3)
Cl, 4*e* (0, 0, *z*)						
z	0.4315(3)	0.4169(1)	0.3818(6)	0.342(6)	0.336(3)	
B (Å^2)	1.88(6)	1.85(7)	1.81(6)	1.52(7)	1.52(7)	
F, 2*a* (0, 0, $^1/_4$)						
Occ.		0.199(1)	0.398(2)	0.607(9)	0.804(5)	1.00
B (Å^2)		1.85(7)	1.81(6)	1.52(7)	1.52(7)	1.46(7)

[a] $R_p = (\sum_i | y_i - y_{ci} |)/\sum_i yi$, $R_{wp} = [(\sum_i w | y_i - y_{ci} |^2)/\Sigma_i w | y_i^2]^{1/2}$, GOF = $\sum_i w (y_i - y_{ci})^2/(n - p)$.

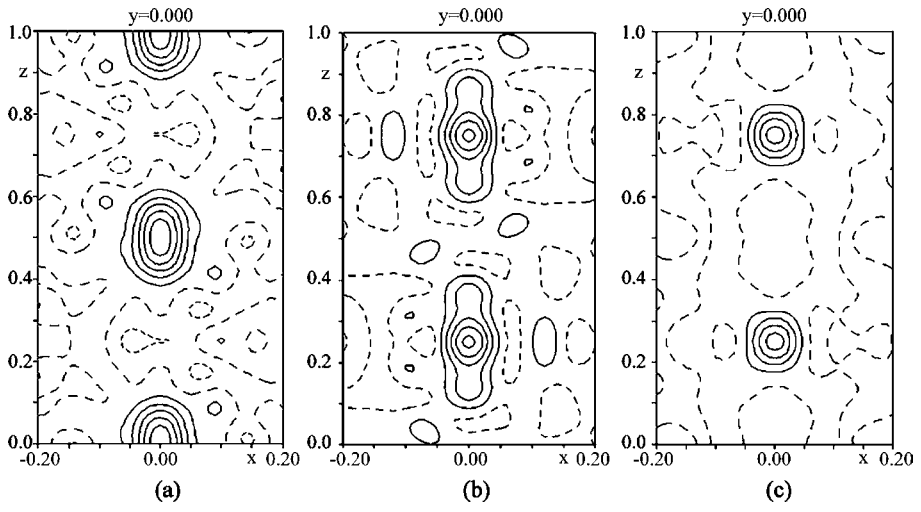

Figure 4. Difference Fourier maps of the $Ca_{10}(SiO_4)_3(SO_4)_3Cl_{2-x}F_x$ ellestadite tunnel indicating the positions of F and/or Cl ions that were excluded to emphasize their location. (a) Chlorellestadite (x = 0), (b) Fluor-chlorellestadite (x = 0.8), and (c) Fluorellstadite (x = 2). Contour interval is 0.5 e/Å^3 and the first positive contour (solid line) is at 0.5 e/Å^3. Negative difference nuclear density is indicated by the broken contours.

dx.doi.org/10.1021/ic201673r | *Inorg. Chem.* 2011, 50, 12641−12650

Table 2. Bond Lengths and Angles for $Ca_{10}(SiO_4)_3(SO_4)_3Cl_{2-x}F_x$

composition x	0	0.4	0.8	1.2	1.6	2.0
Bond Length (Å)						
Ca(1)−O(1) × 3	2.438(3)	2.420(4)	2.419(2)	2.411(5)	2.408(2)	2.405(1)
Ca(1)−O(2) × 3	2.466(3)	2.474(2)	2.475(3)	2.496(5)	2.484(3)	2.491(2)
Ca(1)−O(3) × 3	2.791(3)	2.808(4)	2.815(2)	2.835(5)	2.841(2)	2.834(4)
<Ca(1)-O>	2.565	2.567	2.569	2.580	2.578	2.577
Ca(2)−O(1)	2.893(4)	2.855(1)	2.786(2)	2.726(4)	2.736(3)	2.687(3)
Ca(2)−O(2)	2.283(4)	2.313(1)	2.369(1)	2.400(3)	2.408(3)	2.409(4)
Ca(2)−O(3) × 2	2.582(3)	2.569(2)	2.585(4)	2.574(2)	2.550(1)	2.522(1)
Ca(2)−O(3) × 2	2.358(3)	2.363(1)	2.348(6)	2.353(2)	2.364(2)	2.375(1)
<Ca(2)−O>	2.509	2.505	2.503	2.497	2.495	2.482
Ca(2)−Cl	2.803(4)	2.727(1)	2.589(1)	2.454(1)	2.421(6)	
Ca(2)−F		2.474(1)	2.425(1)	2.370(1)	2.346(6)	2.301(4)
Ca(2)−Ca(2)	4.351(1)	4.286(3)	4.200(6)	4.106(2)	4.063(5)	3.985(5)
Si/S−O(1)	1.544(5)	1.5442(5)	1.544(1)	1.545(5)	1.546(4)	1.5450(1)
Si/S−O(2)	1.545(1)	1.545(1)	1.545(1)	1.545(1)	1.5451(7)	1.5452(1)
Si/S−O(3)	1.545(2)	1.545(1)	1.544(1)	1.5438(2)	1.544(1)	1.5453(6)
average	1.545	1.545	1.544	1.544	1.545	1.545
Angle (degree)						
O(1)-Si/S−O(2)	112.6(2)	112.2(1)	111.4(2)	111.2(2)	111.1(1)	112.027(2)
O(1)−Si/S−O(3)	112.3(2)	112.4(1)	112.2(1)	111.4(2)	111.4(1)	111.04(1)
O(2)−Si/S−O(3)	105.9(2)	106.4(1)	106.4(2)	107.6(2)	108.0(1)	108.016(1)
O(3)−Si/S−O(3)	107.4(1)	106.5(1)	108.06(6)	107.5(1)	106.67(9)	106.469(2)

Table 3. Comparison of Neutron Data Refinement Results Based on Cation Vacancies at Ca(1)/Ca(2), Ca(1) and Ca(2), respectively[a]

		occupancy factor			content per unit cell					
x	vacancy site	Ca(1)	Ca(2)	Cl	Ca	Cl	F	anion vacancy	B (Å^2)	R_B
0	Ca(1)&Ca(2)	0.954(8)	1.000(5)	0.41(2)	9.82	1.64	0	0.36	1.88(6)	2.86
	Ca(1)	0.954(2)	1[b]	0.408(5)	9.82	1.63	0	0.37	1.88(6)	2.86
	Ca(2)	1[b]	0.972(2)	0.416(5)	9.83	1.66	0	0.34	1.92(6)	2.91
0.4	Ca(1)and Ca(2)	0.979(9)	0.967(7)	0.26(2)	9.72	1.04	0.40	0.56	1.85(7)	2.10
	Ca(1)	0.938(3)	1[b]	0.275(7)	9.75	1.10	0.40	0.50	1.86(7)	2.07
	Ca(2)	1[b]	0.952(7)	0.255(4)	9.71	1.02	0.40	0.58	1.85(7)	2.17
0.8	Ca(1)and Ca(2)	0.985(8)	0.988(5)	0.23(2)	9.87	0.94	0.80	0.26	1.81(6)	2.67
	Ca(1)	0.967(3)	1[b]	0.234(6)	9.87	0.94	0.80	0.26	1.82(6)	2.62
	Ca(2)	1[b]	0.978(2)	0.235(5)	9.87	0.94	0.80	0.26	1.82(6)	2.72
1.2	Ca(1) and Ca(2)	1.01(1)	0.977(7)	0.158(3)	9.92	0.63	1.21	0.16	1.52(7)	2.54
	Ca(1)	0.983(3)	1[b]	0.163(7)	9.93	0.65	1.21	0.14	1.55(7)	2.56
	Ca(2)	1[b]	0.987(2)	0.156(7)	9.92	0.63	1.21	0.16	1.53(7)	2.53
1.6	Ca(1) and Ca(2)	1.02(1)	0.989(7)	0.10(3)	10.01	0.40	1.60	0	1.52(7)	2.61
	Ca(1)	1.001(3)	1[b]	0.102(7)	10.00	0.40	1.60	0	1.53(7)	2.63
	Ca(2)	1[b]	0.999(2)	0.098(7)	9.99	0.39	1.60	0.01	1.53(7)	2.62
2.0					10	0	2.0	0	1.46(7)	2.81

[a] $R_b = \sum_i |I_{ko} - I_{kc}| / \sum_i I_{ko}$. [b] Not refined.

SVDdiagnostic,[25] was used to confirm the statistical robustness of the analysis.

2.3. Infrared Spectroscopy. FTIR spectroscopy was used to study the effect of the fluorine substitution on silicate and sulfate absorption bands of ellestadite, and exclude the possible incorporation of CO_3^{2-} and OH^-. Infrared spectra were recorded over the range 400−4000 cm^{-1} with a Fourier Transform Infrared Spectrometer (Perkin-Elmer Spectrum 2000) using the KBr pellet technique, where ellestadite (~1 mg) was ground with oven-dried KBr (200 mg). This homogenized mixture was pressed into 10 mm diameter transparent pellets. Measurements were carried out with a spectral resolution of 4 cm^{-1} and accumulated for 32 scans.

2.4. Transmission Electron Microscopy. Nanometric chemical and structural properties of ellestadite were examined by transmission electron microscopy (TEM). Specimens were prepared by ultrasonically dispersing a small quantity of powder in ethanol then placing a drop of suspension on a holey carbon-coated copper grid dried in air. High-resolution transmission electron microscopy (HRTEM) was carried out at 200 keV with a JEOL 2100F TEM. Samples were orientated with a double tilting holder and the selected area electron diffraction (SAD) patterns recorded. Observation times were limited due to electron amorphization, especially when a more converged beam was used for imaging.

3. RESULTS AND DISCUSSION

3.1. Metalloid Speciation. The incorporation of fluorine did not obviously affect the FTIR spectra of chlorellestadite

dx.doi.org/10.1021/ic201673r | Inorg. Chem. 2011, 50, 12641−12650

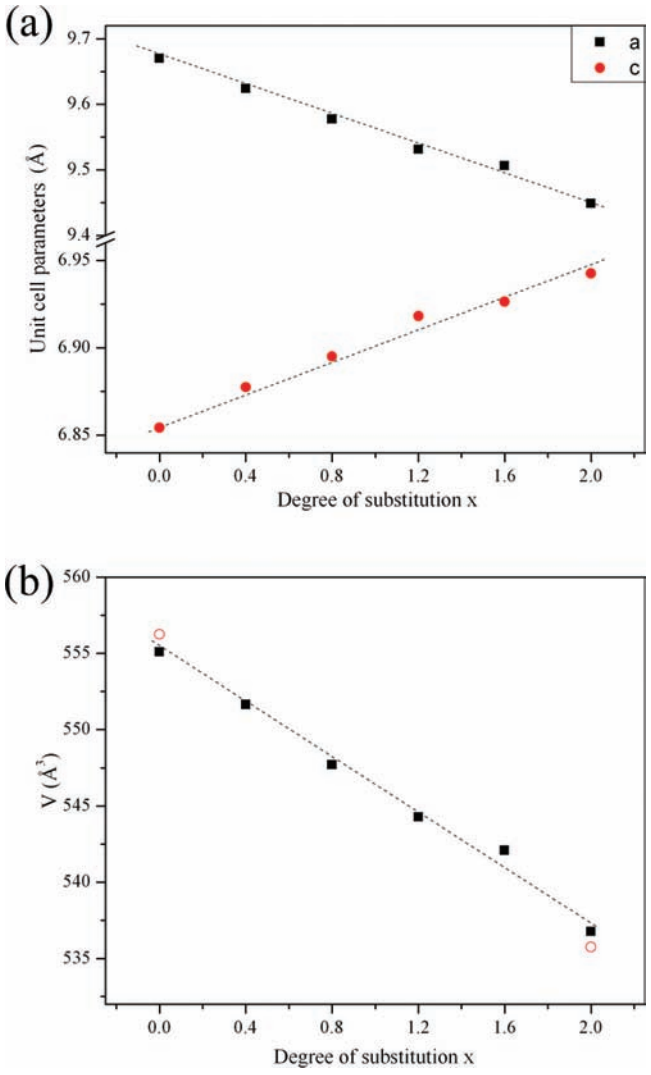

Figure 5. Variation in cell parameters (a) a and c, and (b) unit cell volume with degree of fluorine substitution x in $Ca_{10}(SiO_4)_3(SO_4)_3Cl_{2-x}F_x$. Standard deviation of data is smaller than size of points. The open circles in (b) are taken from the literature[11,12].

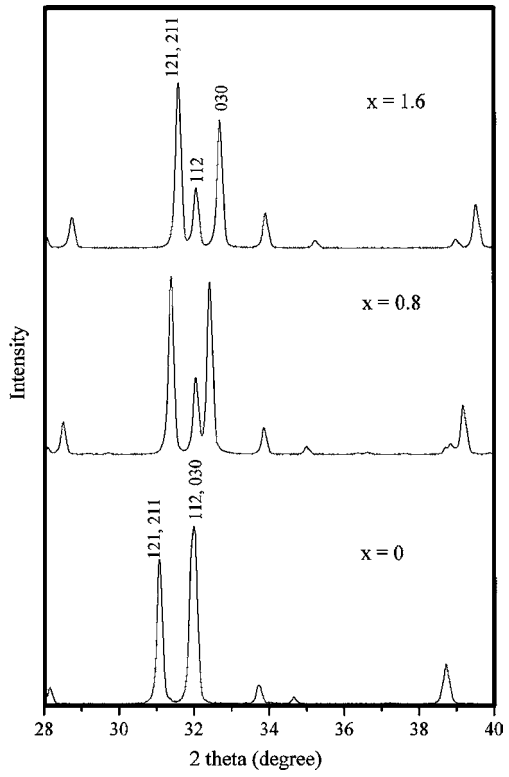

Figure 6. Partial X-ray powder diffraction patterns of ellestadites with x = 0, 0.8, 1.6. (x in $Ca_{10}(SiO_4)_3(SO_4)_3Cl_{2-x}F_x$).

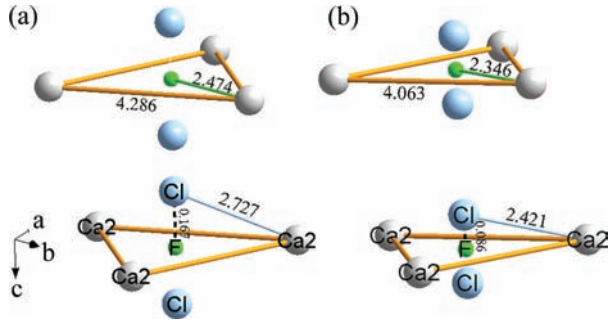

Figure 7. Perspective drawing of Ca(2) triangle arrangement on the screw axis (a) x = 0.4, and (b) x = 1.6. (x in $Ca_{10}(SiO_4)_3(SO_4)_3Cl_{2-x}F_x$) F^- lies in the center of Ca(2) triangle on the mirror planes, while Cl^- splits into two half-occupied sites above or below the mirror plane. The interatomic distances are in Å. The distances between Cl site and the mirror plane (z = $^1/_4$) are indicated by the dotted lines.

(Figure 2). The sulfate ν_3 and ν_4 vibration modes were identified by three features (at 1138, 644, 615 cm^{-1}) as were the silicate ν_3 and ν_4 modes (at 938, 561, 508 cm^{-1}).[26] CO_3^{2-} incorporation, if present, was below the limit of detection. For x = 0.4 and 0.8 (x in $Ca_{10}(SiO_4)_3(SO_4)_3Cl_{2-x}F_x$), the OH^- librational mode appears very weakly at 660 cm^{-1}.

3.2. Quantitative Phase Analysis. Powder XRD shows that ellestadite is always dominant (>95 wt %) (Figure 3). Additionally, the reactants quartz SiO_2 (<0.5 wt %) or anhydrite $CaSO_4$ (<3.5 wt %) persist for low fluorine substituted samples.

3.3. Crystal Structure Analysis. The details of the crystal structure refinements including atomic positional parameters and temperature displacement parameters are given in Table 1, with selected atomic distances and bond angles collected in Table 2. The Rietveld refinement and difference Fourier maps show that across the fluor-chlorellestadite series, the halides occupy the 2a (F^-) or 4e (Cl^-) Wyckoff positions. The location of chlorine ions in the chlorellestadite endmember (x = 0) show nuclear scattering at 4e (0, 0, 0.431), while in fluorellestadite (x = 2), scattering at 2a (0, 0, $^1/_4$) was assigned to F^- (Table 1).

Similar bilocation was used for intermediate F/Cl compositions (Figure 4). The Cl^- position shifts from z = 0.431 in the endmember toward the mirror plane with increasing fluorine content (z = 0.412, 0.382, 0.342, and 0.336 for x = 0.4, 0.8, 1.2, and 1.6, respectively) (Figure 7a). It is likely that the weak OH^- signature observed by FTIR arises from a nonellestadite phase, since a residual feature in the Fourier map cannot be assigned to hydroxyl, as suggested by FTIR for x = 0.4 and 0.8, and if present, OH^- is in low abundance. Examination of the difference Fourier maps (Supporting Information Figure A1) exhibited low electron densities in the range of −0.85 e/Å^3 to 0.85 e/Å^3, which discounts the possibility of multiple Cl^- positions[15] or splitting of Ca(2) site[9] as suggested by earlier studies.

dx.doi.org/10.1021/ic201673r | Inorg. Chem. 2011, 50, 12641−12650

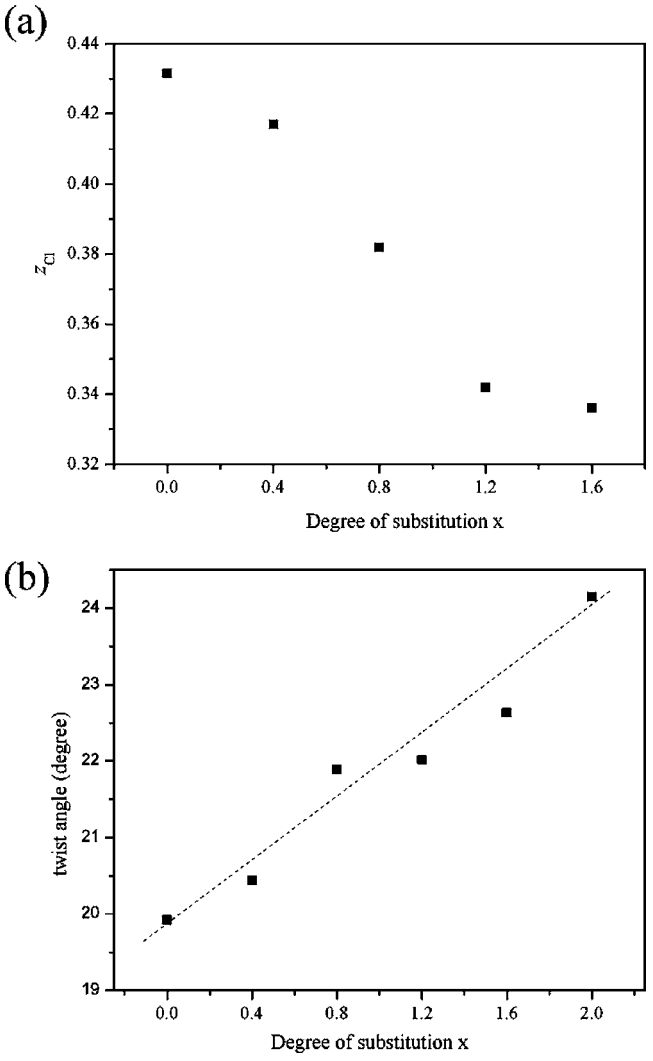

Figure 8. Dependence of (a) z_{Cl} and (b) twist angle on degree of fluorine substitution x in $Ca_{10}(SiO_4)_3(SO_4)_3Cl_{2-x}F_x$.

The Cl content was less than nominal for samples with $x \leq 1.2$. Halogen loss might occur during the solid state processing, as chlorine is susceptible to volatilisation, with possible charge compensation mechanisms being

$$Cl^- \rightarrow OH^- \quad (1)$$

$$Cl^- \rightarrow O^{2-} + \square_{Cl} \quad (2)$$

$$Ca^{2+} + 2Cl^- \rightarrow \square_{Ca} + 2\square_{Cl} \quad (3)$$

Mechanism 1 is not supported by FTIR or structure refinement. In the case of mechanism 2, attempts to insert extra oxygen at additional (0, 0, z) positions on the hexagonal axis were unsuccessful, as the temperature displacement parameter of oxygen atom became negative. Prener[27] studied nonstoichiometry in calcium chlorapatite, and stated that synthetic chlorapatite (often $P2_1/b$) became hexagonal $P6_3/m$ when grown from the melt due to Cl deficiency created by loss of $CaCl_2$. In our study, the formation of Ca and Cl structural vacancies (mechanism 3) is possible as $CaCl_2$ partially evaporates during sintering at 950 °C ($m_p(CaCl_2)$ = 782 °C). This would be consistent with the smaller unit cell parameter a (9.6702(3) Å) and volume (555.09(4) Å^3) of the chlorellestadite endmember, compared with stoichiometric chlorellestadite (a = 9.6773(3) Å, V = 556.25(4) Å^3) reported previously.[9] To examine this question, the occupancies of calcium and chlorine were refined with the constraint $Ca^{2+} + 2Cl^- \rightarrow \square_{Ca} + 2\square_{Cl}$ applied in three ways: (i) the occupancies of Ca(1) and Ca(2) were jointly refined together with Cl, (ii) the Ca(1) site was constrained with Cl site, with the Ca(2) site fully occupied, and (iii) the Ca(2) site was released with Ca(1) fixed to full occupancy. In this way, any preference to create Ca-site vacancies within the framework or tunnel could be distinguished (Table 3). While the differences in refinement residuals are small, it does appear that for Cl-rich compositions, Ca(1) vacancies may be present, while for F-rich ellestadites the reverse is true. However, further analysis would be required. It is noted that modeling with the Ca(1) and Ca(2) sites fully occupied lead to substantially inferior residuals, and in addition, cannot charge balance halogen substoichiometry. On the basis of these assessments, the formulas for these compounds are most generally written as $Ca_{10-y}(SiO_4)_3(SO_4)_3Cl_{2-x-2y}F_x$, rather than the nominal $Ca_{10}(SiO_4)_3(SO_4)_3Cl_{2-x}F_x$.

Singular value decomposition (SVD) as adapted by Mercier et al.[25,28] for the evaluation apatite structures, found the numerical stability of the Rietveld refinements was satisfactory: in particular, the tunnel site occupancy was reliable. Typical outputs (Supporting Information Table A1) from *SVDdiagnostic* of the preconditioned normal matrices for the models in which the Ca(1) and Ca(2) sites were refined simultaneously (see also Table 3), give condition numbers of around 10^2–10^3 indicative of good conditioning of the least-squares matrices, that confirms the occupancy factors refinements are reasonable and not over interpreted. Similar results were obtained if Ca(1) or Ca(2) were refined alone.

As the content of fluorine increases, a contracts while c dilates, but overall the unit cell volume is reduced (Table 1, Figure 5), because fluorine is smaller than chlorine. In addition, the splitting of the intense doublet reflections (121)/(211) and (112)/(030) in the chlorellestadite endmember pattern into a resolved triplet (121)/(211), (112), and (030) provides further confirmation of the mixed anion structure[21] (Figure 6). The loss of $CaCl_2$ from the structure also contributes to unit cell shrinkage. According to Young and Elliott,[29] the small increase in c may be related to the different atomic positions of halogen ions. As fluorine is centered in the Ca(2) triangle ($z = {}^1/_4$), it will not affect the c axes. However, chlorine is displaced >1 Å along c, weakly bonding to the neighboring calcium Ca(2) triangles that leads to slight contraction of the c axis.

Differences in the anion content of the tunnel negligibly disturbs the $(Si/S)O_4$ tetrahedra, which are essentially rigid bodies, and the $Ca(1)O_9$ polyhedra (Table 2). There are only minor changes in the (Si/S)–O bond lengths and no evidence for a Si/S ordering which would lower the symmetry to monoclinic. The refined mean bond length Si/S–O = 1.545 Å, close to the average value of 1.55 Å calculated from Si–O = 1.61 Å in silicates[30] and S–O = 1.49 Å in sulphates,[31] is also consistent with a statistical distribution of SiO_4 and SO_4 tetrahedra.

The major structural response to fluorine substitution occurs in the $Ca(2)O_5(F/Cl)(O)$ polyhedron (a seventh weak bond to O(1) exists in fluorellestadite) (Table 2). As noted the Ca(2) atoms located on the mirror planes at $z = {}^1/_4$ and ${}^3/_4$ form triangles that are centered around the [001] $\bar{3}$ axis containing the F/Cl (Figure 7). The Cl^- ion located in 4*e* shifts from z = 0.4315(3) in the chlorellstadite endmember toward the Ca(2) triangles as z decreases to 0.336(3) (Figure 8a).

dx.doi.org/10.1021/ic201673r | *Inorg. Chem.* 2011, 50, 12641–12650

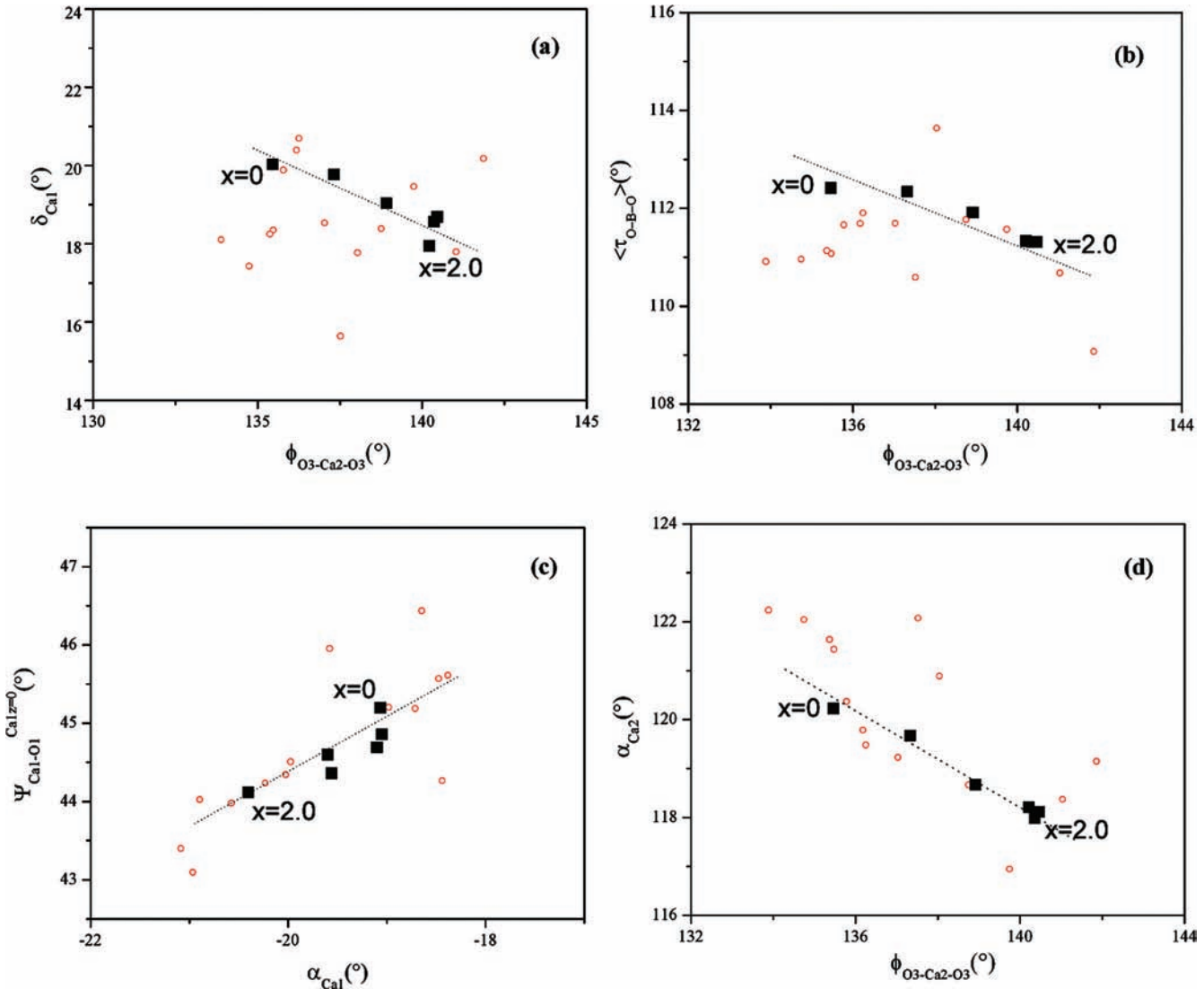

Figure 9. Correlations observed between polyhedral distortion parameters: (a) δ_{Ca1} versus $\phi_{O3-Ca2-O3}$, (b) $<\tau_{O-B-O}>$ versus $\phi_{O3-Ca2-O3}$, (c) $\Psi_{Ca1-O1}^{Ca1\ z=0}$ versus α_{Ca1}, and (d) α_{Ca2} versus $\phi_{O3-Ca2-O3}$. These figures should be compared with Figure.8 in Mercier et al.[33] Circles: published data; large filled squares: this study. (δ_{Ca1}:counter-rotation angle of CaO_6 polyhedra; $\phi_{O3-Ca2-O3}$: O3−Ca2−O3 bond angle; $<\tau_{O-B-O}>$: O−B−O bond-bending angle; $\Psi_{Ca1-O1}^{Ca1\ z=0}$: angle that an $Ca1_{z=0}$−O1 bond makes with respect to *c*; α_{Ca1}: orientation of CaO_6 polyhedra with respect to *a*; α_{Ca2}: orientation of Ca2 triangles with respect to *a*.).

The interatomic distances between Ca(2) and Cl decreased from 2.803(4) Å in the chlorellestadite (x = 0) to 2.421(6) Å when x = 1.6. The Ca(2)-F bond length also follows this trend, decreasing from 2.474(5) Å in x = 0.4 to 2.3018(1) Å in fluorellestadite (x = 2.0) (Table 2). As the F^- ion lies in the center of the Ca(2) triangle, the decrease of the Ca(2)−F distances with reduction of chlorine content leads to a contraction in the unit cell *a*-parameter (Table 1, Figure 5b).

The metaprism twist angle (φ), defined as the (001) projected angle of the O(1)−Ca(1)−O(2), was used to validate the Rietveld refined ellestadite structures (Table 2). The twist angle (φ) is related to the relative sizes of the *A*, *B*, and *X* ions[32] and also sensitively detects disequilibrium and nonstoichiometry. In passing from fluorellestadite (x = 2) to chlorellestadite (x = 0), the twist angle (φ) decreases from 24.1° to 19.9°, with increasing chlorine content leading to a tunnel dilation and to increased Ca(2)−F/Cl distances. The near linear change in twist angle (φ) is expected, and small departures from linearity may be indicative of Cl deficient nature of some compositions (Figure 8b).

As further validation of the refined structures, the crystal-chemical parameters proposed by Mercier et al.[33] (Supporting Information Table A2) were extracted for the refined ellestadite structures; the geometrical derivation of these parameters can be found in this earlier work. The principle correlations among those crystal-chemical parameters, including data from this study and published work are shown in Figure 9. As the fluorine content increases, the $(Si/S)O_4$ tetrahedra ($\tau_{O3-Ca2-O3}$ decreases) and CaO_6 polyhedra (δ_{Ca1} decreases) are distorted to accommodate the increase of the O3−Ca2−O3 bond angle ($\phi_{O3-Ca2-O3}$). These correlations conform to the trends observed by Mercier et al.[33] (Figure 8 in ref 33.), and of particular interest, fill a gap noted in their work for apatites with $131° < \phi_{O3-Ca2-O_3} < 135°$. Furthermore, the crystal chemical parameters are clustered for F-rich compositions consistent with loss of Cl, and confirm there is little change in halide content for these materials.

dx.doi.org/10.1021/ic201673r | *Inorg. Chem.* 2011, 50, 12641−12650

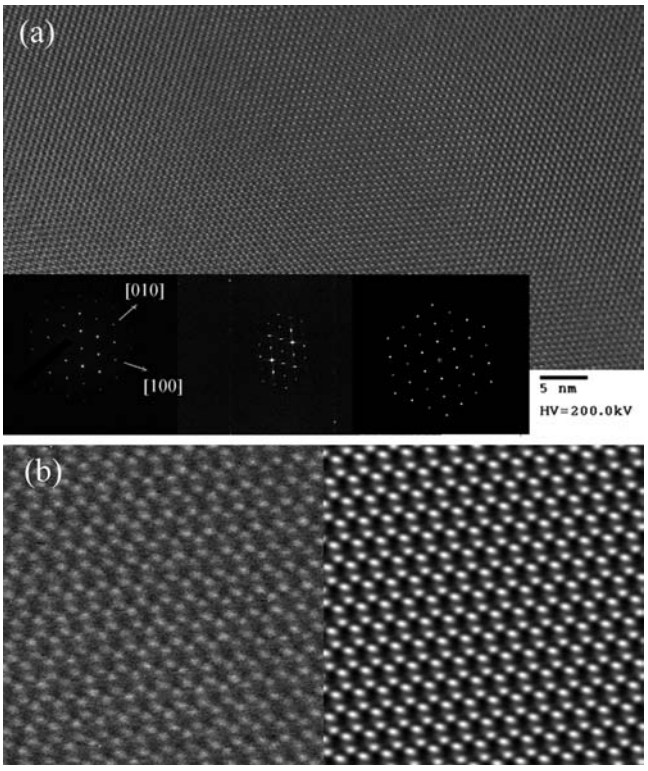

Figure 10. (a) Wide field [001] HRTEM image of $Ca_{10}(SiO_4)_3(SO_4)_3Cl_{0.4}F_{1.6}$, (experimental, FFT and simulated SAED reflections are provided.) (b) The as-collected images (left) and processed image (right) constrained by *p6* symmetry are shown.

None of the ellestadites show measurable deviation from the hexagonal metric. This behavior is distinct from the $Ca_{10}(V_xP_{1-x}O_4)_6F_2$ apatites,[34] which at the largest vanadium contents become triclinic. For these materials, the approach of α_{Ca2} to 120° was seen to precede a reduction in symmetry. However, in this study it was found that $Ca_{10}(SiO_4)_3(SO_4)_3Cl_2$ with α_{Ca2} = 120.23° could be convincingly modeled in $P6_3/m$. It has already been noted that mineral ellestadites may be monoclinic, and long annealing of synthetic $Ca_{10}(SiO_4)_3(SO_4)_3Cl_2$ may allow SiO_4/SO_4 ordering with stabilization as $P2_1/m$ or $P2_1$ structures.

3.4. Local Structure. A high-resolution TEM image of $Ca_{10}(SiO_4)_3(SO_4)_3Cl_{0.4}F_{1.6}$ shows a well developed crystal without obvious imperfection, in the sense that no extended defects are observed (Figure 10a). A comparison of the intensity distribution of experimental and simulated SAED reflections was consistent with $P6_3/m$ symmetry. The SAED pattern did not show split reflections, precluding the possibility of coexisting mixed-phase ellestadite,[19] or localized order with respect to anionic sequences within the anion tunnels that would lower the symmetry to monoclinic. Fourier reconstruction of the images yield potential maps (Figure 10b) most plausibly constrained to the plane group *p6* which is the [001] symmetry projection for $P6_3/m$. In the HR image, the darker feature represents the positions of $Ca(1)O_9$ polyhedral columns which share (001) pinacoid faces to form chains parallel to *c*, while the bright contrast corresponds to the anion columns at the tunnel centers.

4. CONCLUSION

The synthesis of fluorine-substituted chlorellestadites has been achieved by the solid state method, and the crystal structures refined via powder X-ray and neutron diffraction using $P6_3/m$ symmetry. Ordering of the Si and S atoms within the tetrahedra, or halides between the tunnels can be excluded, as this would lead to $P2_1/m$ or $P2_1/b$ structures respectively, with a possible doubling of the unit cell in the *a* or *b* directions. In natural ellestadites, described in $P2_1/m$ and $P2_1$, equilibration over very long geological periods may favor lower symmetry. For the synthetic ellestadites studied here, increasing fluorine content, leads to a progressive shift of Cl^- toward the center of the Ca(2) triangle; the formation of a shorter, stronger bond between Ca(2) and Cl may enhance the chemical stability of ellestadite. Minor loss of $CaCl_2$ during sintering induces Ca-vacancies within ellestadite that was confirmed by powder neutron diffraction, and verified by the spread of $Ca(1)O_6$ metaprism twist angles as a function of composition, although the overall trend is linear. For charge balance, halide vacancies in the anion tunnel were compensated by calcium vacancies, and may be required to provide structural accommodation for larger Cl ions, or reduce structural strain due to the mismatch of the framework and tunnel dimensions. The reliability of Rietveld refinements were evaluated by Singular Value Decomposition and correlations of various crystal−chemical parameters. Future reports will focus on compositionally complex ellestadites and chemical tailoring that improves the stability and effectiveness of waste form ceramics.

■ ASSOCIATED CONTENT

Ⓢ Supporting Information

Examples of the output of *SVDdiagnostic* of Rietveld refinements of ellestadites, crystal-chemical parameters extracted from the crystallographic descriptions, neutron crystallographic files in CIF format, experimental and calculated powder X-ray and neutron diffraction patterns, difference Fourier map of nuclear density for $Ca_{10}(SiO_4)_3(SO_4)_3Cl_{0.8}F_{1.2}$, and bond-valence sums (BVS) at site Ca1 and Ca2 plotted as a function of the degree of fluorine substitution *x*, *x* in $Ca_{10}(SiO_4)_3(SO_4)_3Cl_{2-x}F_x$. This material is available free of charge via the Internet at http://pubs.acs.org.

■ AUTHOR INFORMATION

Corresponding Author

*E-mail: fang0027@e.ntu.edu.sg.

■ ACKNOWLEDGMENTS

Yanan Fang thanks Nanyang Technological University, Singapore, for the NTU Research Scholarship supporting this study.

■ REFERENCES

(1) Dong, Z.; White, T. J.; Wei, B.; Laursen, K. *J. Am. Ceram. Soc.* **2002**, *85*, 2515−2522.
(2) Nishikawa, H.; Omamiuda, K. *J. Mol. Catal.* **2002**, *179*, 193−200.
(3) Driessens, F. C. M.; Verbeeck, R. M. H. *J. Cryst. Growth* **1981**, *53* (1), 55−62.
(4) Hertz, A.; Bruce, I. J. *Nanomedicine* **2007**, *2* (6), 899−918.
(5) Neubauer, J.; Erlangen, H. P. *N. Jb. Miner. Abh.* **1995**, *168* (3), 237−258.
(6) McConnell, D. *Am. Mineral.* **1937**, *22*, 977−986.
(7) Sudarsanan, K. *Acta Cryst. B: Struct. Sci.* **1980**, *36*, 1636−1639.
(8) Organova, N. I.; Rastsvetaeva, R. K.; Kuz'mina, O. V.; Arapova, G. A.; Litsarev, M. A.; Fin'ko, V. I. *Kristallografiya* **1994**, *39*, 278−282.

(9) Saint-Jean, S. J.; Sweden, S. H. *Solid State Sci.* **2005**, *7*, 97−102.
(10) Dean, H. T. *Public Health Rep. Wash.* **1938**, *53*, 1443−1452.
(11) Lexa, D. *Metall. Mater. Trans.* **1999**, *30A*, 147−153.
(12) Pajares, I.; de la Torre, Á. G.; Martínez-Ramírez, S.; Puertas, F. *Powder Diffr.* **2002**, *17*, 281−286.
(13) Shannon, R. D. *Acta Crystallogr., Sect. A: Cryst. Phys., Diffr., Theor. Gen. Crystallogr.* **1976**, *32*, 751−767.
(14) Onac, B. P.; Effenberger, H.; Ettinger, K.; Panzaru, S. C. *Am. Mineral.* **2006**, *91*, 1927−1931.
(15) Hughes, J. M.; Rakovan, J. *Rev. Mineral. Geochem.* **2002**, *48* (1), 1−12.
(16) Mccubbin, F. M.; Mason, H. E.; Park, H.; Phillips, B. L.; Parise, J. B.; Nekvasil, H.; Lindsley, D. H. *Am. Mineral.* **2008**, *93*, 210−216.
(17) Mackie, P. E.; Young, R. A. *J. Solid State Chem.* **1974**, *11*, 319−329.
(18) Hughes, J. M.; Cameron, M.; Crowley, K. D. *Am. Mineral.* **1990**, *75*, 295−304.
(19) Ferraris, C.; T. J. White, T. J.; Plévert, J.; Wegner, R. *Phys. Chem. Mineral* **2005**, *32*, 485−492.
(20) Bruker. TOPAS Version 3, Bruker AXS Inc., Madison, WI, USA, 2005.
(21) Saint-Jean, S. J.; JØns, E.; Lundgaard, N.; Hansen, S. *Cem. Concr. Res.* **2005**, *35*, 431−437.
(22) Sears, V. F. In *International Tables for Crystallography*; Wilson, A. J. C., Ed.; Kluwer Academic Publishers: Dordrecht, 1993; Vol. *C*, p 383.
(23) Petricek, V.; Dusek, M.; Palatinus, L. *Jana2006. The Crystallographic Computing System*; Institute of Physics: Praha, Czech Republic. 2006.
(24) White, T. J.; Dong, Z. L. *Acta Cryst. B: Struct. Sci.* **2003**, *59*, 1−16.
(25) Mercier, P. H. J.; Le Page, Y.; Whitfield, P. S.; Mitchell, L. D. *J. Appl. Crystallogr.* **2006**, *39*, 458−465.
(26) Griffith, W. P. *Nature* **1969**, *224*, 264−266.
(27) Prener, J. S. *J. Solid State Chem.* **1971**, *3*, 49−55.
(28) Mercier, P. H. J.; Le Page, Y.; Whitfield, P. S.; Mitchell, L. D. *J. Appl. Crystallogr.* **2006**, *39*, 369−375.
(29) Young, R. A.; Elliott, J. C. *Archs. Oral. Biol.* **1966**, *11*, 699−707.
(30) Smith, J. V.; Baily, S. W. *Acta Crystallogr.* **1963**, *16*, 801−811.
(31) Wuench, B. J. Sulfur, 16-A Crystal chemistry. In*Handbook of Geochemistry*; Wedepohl, K. H., Ed.; Springer-Verlag: Berlin, 1970; Vol. *II/2*, 16A, pp 1−19.
(32) White, T. J.; Ferraris, C.; Kim, J.; Madhavi, S. *Rev. Mineral. Geochem.* **2005**, *57*, 307−401.
(33) Mercier, P. H. J.; Le Page, Y.; Whitfield, P. S.; Mitchell, L. D.; Davidson, I. J.; White, T. J. *Acta Cryst. B: Struct. Sci.* **2005**, *61*, 635−655.
(34) Mercier, P. H. J.; Dong, Z.; Baikie, T.; le Page, Y.; White, T. J.; Whitfield, P. S.; Mitchel, L. D. *Acta Cryst. B: Struct. Sci.* **2007**, *63*, 37−48.